Active Reconfigurable Intelligent Surface Assisted Near-Field Covert-Overt Communications

Ruby Jane Pedronan Agullana[†], Keshav Singh[†,‡], Arnav Mukhopadhyay[‡], Hyundong Shin[§] and Trung Q. Duong[*]
[†]IMPTE, National Sun Yat-sen University, Kaohsiung, Taiwan
[‡]Institute of Communications Engineering, National Sun Yat-sen University, Kaohsiung, Taiwan
[§]Department of Electronics and Information Convergence Engineering, Kyung Hee University, Republic of Korea
[*]Faculty of Engineering and Applied Science, Memorial University, St. John's, NL A1C 5S7, Canada
Email: {rubyjaneagullana, gudduarnav}@gmail.com, hshin@khu.ac.kr, ksingh@ieee.org, tduong@mun.ca

***Abstract*—This paper investigates a joint beamforming and reflection vector optimization for an active reconfigurable intelligent surface (RIS) to enhance overt–covert communications in sixth-generation (6G) near-field (NF) networks. We consider a multi-antenna base station that simultaneously serves multiple covert users (Bobs) and overt users (Carols) with the aid of an electrically-powered RIS capable of signal amplification and phase control. To guarantee low-probability-of-detection, a tractable covertness constraint is derived by coupling Kullback-Leibler (KL) divergence with Pinsker's inequality under worst-case channel-state-information (CSI) uncertainty at the eavesdropper (Willie). The ensuing weighted sum-rate maximization problem, subject to quality of service (QoS), transmit-power budgets, RIS hardware limits, and the covert constraint highly non-convex. To address the inherent non-convexity of the joint design problem, we employ an alternating optimization (AO) framework wherein each subproblem is reformulated and efficiently solved via successive convex approximation (SCA), and second-order cone programming (SOCP) regularized by penalty terms that converge to a stationary point with polynomial complexity. Numerical results at 40 dBm and 24 GHz show that the proposed NF algorithm achieves up to $24\,nat/s/Hz$ aggregate throughput—more than triple far-field (FF) or passive-RIS baselines, while keeping Willie's total variation distance (TVD) low to ensure covertness across diverse power budget, even under severe CSI errors at willie, confirming the efficacy of active RIS and NF focusing for practical 6G covert communication.**

***Index Terms*—Active RIS, covert communications, KL divergence, near-field beamforming, robust optimization.**

I. Introduction

WIRELESS communication technologies have rapidly advanced, giving rise to sixth-generation (6G) networks that promise ultra-low latency, terabit-per-second data rates, and massive device connectivity to meet the growing demands of dense networks and the Internet of Things (IoT) [1]. However, the inherent broadcast nature of wireless channels introduces significant security vulnerabilities, including eavesdropping and information leakage [2]. Traditional methods primarily safeguard content; however, emerging threats require solutions that obscure the transmission itself, spurring interest in covert communication techniques.

Covert communication emphasizes undetectability, complementing conventional security and differing from physical layer security (PLS), which focuses on making data unintelligible through channel characteristics. In contrast, covert communication aims to obscure the existence of transmission itself, a capability that is essential for stealth-critical 6G applications. A key milestone is the "square-root-law" [3], which limits covert throughput over Additive White Gaussian Noise (AWGN) channels to $\mathcal{O}(\sqrt{n})$ bits across n uses channels. To surpass this bound, researchers have investigated relaxed constraints and auxiliary resources. For instance, [4] and [5] extended covert analysis to discrete memoryless channels (DMCs), though practical implementation remains challenging due to wideband spectrum and memoryless requirements. Alternatively, [6] employed antenna selection to enhance signal-to-interference-plus-noise ratio (SINR) for legitimate users while degrading it at eavesdroppers, and [7] introduced dual-functional artificial noise (DFAN) to mask transmissions by overpowering eavesdroppers with noise while aiding localization. Relay-based methods [8] and cooperative jamming [9] further confuse adversaries by exploiting channel uncertainty or power allocation, often enforcing Kullback-Leibler (KL) divergence constraints to limit detection probability. More recently, Reconfigurable Intelligent Surfaces (RIS) have emerged as a key enabler for covert communication by dynamically shaping wireless propagation, favoring legitimate users and impairing eavesdroppers [10]. Compared to traditional relays, RIS offers energy-efficient, low-cost solutions for coverage extensions and spectral efficiency, aligning with the demands for covert scenarios [11]. Furthermore, active RIS equipped with amplification capabilities provides additional control over signal power and direction, offering enhanced opportunities for covertness [12].

Building on recent developments, this paper investigates RIS under a near-field (NF) propagation model, where spatial focusing and amplification are leveraged to enhance both throughput and covert performance, surpassing traditional far-field (FF) assumptions [13]. Robust system design is critical under channel state information (CSI) uncertainty, modeled using bounded error sets, as inaccuracies in CSI can significantly degrade performance [12]. Existing approaches often employ linear matrix inequalities (LMI) methods to manage CSI uncertainty [9]; however, their computational burden limits scalability to large-scale systems. To address this, we propose a successive convex approximation (SCA) and second-order

This work was supported by the National Science and Technology Council of Taiwan under Grants NSTC 114-2218-E-110-005 and NSTC 112-2221-E-110-038-MY3.

cone programming (SOCP). In this framework, SCA iteratively approximates nonconvex constraints with convex surrogates, ensuring convergence to a stationary solution, while SOCP efficiently solves the resulting subproblems [14]. This approach substantially reduces computational complexity and enhances scalability, making it more suitable for practical 6G networks with large antenna arrays and RIS elements deployments. In addition to this, penalty formulations are incorporated to maintain solution feasibility and prevent divergence from the approximated solution space. In practical 6G networks, ensuring undetectable sensitive transmissions is as critical as maximizing data rates. However, most covert communication designs assume FF propagation and passive RIS, neglecting the spatial focusing and amplification benefits of NF active RIS. To address this, we propose a robust joint beamforming and active RIS design that enhances user rates and covertness under bounded CSI uncertainty at the eavesdropper, making covert communication feasible under realistic 6G conditions.

The main contributions of this work are as follows: We propose an NF-based overt–covert communication system empowered by an active RIS that enables simultaneous signal amplification and spatial beam shaping. To ensure covertness, a tractable constraint is derived using the KL divergence and Pinsker's inequality, accounting for bounded uncertainty in Willie's channel. We formulate a robust joint beamforming and active RIS optimization problem and solve it via an alternating optimization framework, where each subproblem is convexified using SOCP-based SCA. Extensive simulations demonstrate that the proposed design significantly outperforms Particle Swarm Optimization (PSO) based heuristics, particularly under CSI uncertainty and practical RIS power constraints.

II. System Model

Consider the system model depicted in Fig. 1, where a base station Alice is equipped with a uniform planar array (UPA) of $N \times N$ antenna elements. Alice concurrently serves two classes of users, B covert receivers (Bobs) and C overt receivers (Carols). A uniform planar active diagonal RIS with $M \times M$ elements is deployed to enhance signal coverage and spectral efficiency. Meanwhile, an eavesdropper, Willie, attempts to detect covert communication between Alice and the Bobs, disregarding transmissions to the Carols. Hence, the design objective of the considered network is twofold: to minimize the detectability of covert transmissions at Willie, thereby ensuring covertness, and to jointly optimize the fair rate allocation among Bobs and Carols, subject to quality-of-service (QoS) constraints for both the direct and RIS-assisted links.

A. Signal Model

Transmitted Signal: Let $s_b^{\mathcal{B}}(t) \sim \mathcal{CN}(0,1)$ and $s_c^{\mathcal{C}}(t) \sim \mathcal{CN}(0,1)$ denote the unit-energy signal intended for b-th Bob and c-th Carol, respectively. These signals satisfy the power normalization conditions $\mathbb{E}\left[s_b^{\mathcal{B}} s_b^{\mathcal{B}^*}\right] = \mathbb{E}\left[s_c^{\mathcal{C}} s_c^{\mathcal{C}^*}\right] = 1$. Each symbol is precoded using a dedicated beamforming vectors $\mathbf{w}_b^{\mathcal{B}}, \mathbf{w}_c^{\mathcal{C}} \in \mathbb{C}^{N^2 \times 1}$. Accordingly, the transmitted signal $\mathbf{x}(t)$ can be modeled under two transmission scenarios: *null hypothesis* ($\mathcal{H}_0$) to represent only overt transmission and *alternative hypothesis* ($\mathcal{H}_1$) to indicate the presence of covert communication. The resulting transmit signal model is given by

$$\mathbf{x}(t) = \begin{cases} \sum_{c=1}^{C} \mathbf{w}_c^{\mathcal{C}} s_c^{\mathcal{C}}(t), & \mathcal{H}_0 \\ \sum_{b=1}^{B} \mathbf{w}_b^{\mathcal{B}} s_b^{\mathcal{B}}(t) + \sum_{c=1}^{C} \mathbf{w}_c^{\mathcal{C}} s_c^{\mathcal{C}}(t), & \mathcal{H}_1. \end{cases} \tag{1}$$

To simplify the notation, the signal expression can be rewritten in matrix form as

$$\mathbf{x}(t) = \begin{cases} \mathbf{W}^{\mathcal{C}} \mathbf{s}^{\mathcal{C}}, & \mathcal{H}_0 \\ \mathbf{W}^{\mathcal{B}} \mathbf{s}^{\mathcal{B}} + \mathbf{W}^{\mathcal{C}} \mathbf{s}^{\mathcal{C}}, & \mathcal{H}_1, \end{cases} \tag{2}$$

where $\mathbf{W}^{\mathcal{B}} = \left[\mathbf{w}_1^{\mathcal{B}}, \cdots, \mathbf{w}_B^{\mathcal{B}}\right] \in \mathbb{C}^{N^2 \times B}$ and $\mathbf{W}^{\mathcal{C}} = \left[\mathbf{w}_1^{\mathcal{C}}, \cdots, \mathbf{w}_C^{\mathcal{C}}\right] \in \mathbb{C}^{N^2 \times C}$ are the beamforming matrix for Bobs and Carols, respectively. $\mathbf{s}^{\mathcal{B}} = \left[s_1^{\mathcal{B}}, \cdots, s_B^{\mathcal{B}}\right]$ and $\mathbf{s}^{\mathcal{C}} = \left[s_1^{\mathcal{C}}, \cdots, s_C^{\mathcal{C}}\right]$ denote the composite symbol vectors.

RIS-Reflected Signal Model: The signal reflected by the active RIS at time instant t is modeled as

$$\mathbf{x}^{\mathcal{R}}(t) = \mathbf{\Theta} \mathbf{G} \mathbf{x}(t) + \mathbf{\Theta} \mathbf{z}_{\mathcal{R}}(t), \tag{3}$$

where $\mathbf{G} \in \mathbb{C}^{M \times N^2}$ denotes the channel matrix between Alice and the active RIS, $\mathbf{z}_{\mathcal{R}} \sim \mathcal{CN}\left(0, \text{diag}\left(\sigma_{\mathcal{R}}^2 \mathbf{I}_M\right)\right) \in \mathbb{C}^{M \times 1}$ represents the AWGN introduced by the active RIS, and $\mathbf{\Theta} = \text{diag}\{\phi_1, \cdots, \phi_m\} \in \mathbb{C}^{M \times M}$, is a diagonal reflection matrix, where each diagonal entry ϕ_m models the complex reflection coefficient at the m-th RIS element. Specifically, each reflection coefficient ϕ_m simultaneously adjusts both the amplitude and phase of the incident signal. The phase shift satisfies $\arg \phi_m \in [0, 2\pi)$ while the amplitude gain is constrained to the following bound [15]

$$1 \leq |\phi_m| \leq \eta^{\mathcal{R}}, \quad \forall\, m = 1, 2, \cdots, M, \tag{4}$$

where $\eta^{\mathcal{R}^2}$ indicates the maximum allowable power amplification factor for the m-th RIS element.

Power Budget: The majority of power consumption within the wireless network arises from two principal sources: the base station (Alice) and the active RIS. At Alice, the power is consumed primarily due to the transmission of beamformed signals. The total power is constrained as follows:

$$||\mathbf{W}^{\mathcal{B}}||_F^2 + ||\mathbf{W}^{\mathcal{C}}||_F^2 \leq P_T^{\mathcal{A}}, \tag{5}$$

where $||\mathbf{W}^{\mathcal{B}}||_F^2$ and $||\mathbf{W}^{\mathcal{C}}||_F^2$ denote the transmit power allocated for beamforming vectors targeting Bob and Carol, respectively, and $P_T^{\mathcal{A}}$ represents Alice's total power budget.

Similarly, the active RIS consumes power to amplify and reflect the incident signals. Its total power consumption comprises three components and can be written as [15]

$$||\mathbf{\Theta} \mathbf{G} \mathbf{W}^{\mathcal{B}}||_F^2 + ||\mathbf{\Theta} \mathbf{G} \mathbf{W}^{\mathcal{C}}||_F^2 + ||\mathbf{\Theta}||_F^2 \sigma_{\mathcal{R}}^2 \leq P_T^{\mathcal{R}}, \tag{6}$$

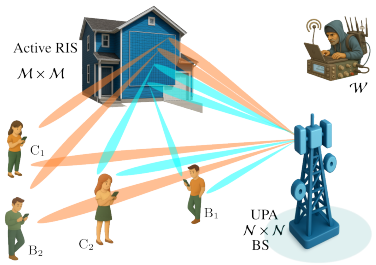

Fig. 1: Active-RIS-assisted NF covert/overt network model.

where $||\mathbf{\Theta}||$ is the diagonal reflection matrix, $\sigma_{\mathcal{R}}^2$ is the noise introduced by active components of the RIS, and $P_T^{\mathcal{R}}$ is the maximum allowable power budget.

B. Recieved Signals

The received signal at k-th node is given by

$$y_k^{\mathcal{K}}(t)=\left(\mathbf{h}_k^{\mathcal{AK}}+\mathbf{h}_k^{\mathcal{RK}}\mathbf{\Theta}\mathbf{G}\right)\mathbf{x}(t)+\mathbf{h}_k^{\mathcal{RK}}\mathbf{\Theta}\mathbf{z}_{\mathcal{R}}(t)+z_k^{\mathcal{K}}(t), \quad (7)$$

where $k \in \{b,c,w\}$ and $K \in \{\mathcal{B},\mathcal{C},\mathcal{W}\}$. $\mathbf{h}_k^{\mathcal{AK}} \in \mathbb{C}^{1\times N^2}$ denotes the direct channel from Alice to k-th node, $\mathbf{h}_k^{\mathcal{RK}} \in \mathbb{C}^{1\times M}$ represents the RIS-assisted reflected channel, and $z_k^{\mathcal{K}}(t) \sim \mathcal{CN}\left(0,\sigma_k^{\mathcal{K}^2}\right)$ is the AWGN at k-th node.

C. Achievable Rate Throughput

Achievable Rate at Bobs: Consider the effective channel for the b-th Bob as follows:

$$\mathbf{h}_b^{\mathcal{B}}=\mathbf{h}_b^{\mathcal{AB}}+\mathbf{h}_b^{\mathcal{RB}}\mathbf{\Theta}\mathbf{G}, \quad \mathbf{h}_b^{\mathcal{B}} \in \mathbb{C}^{1\times N^2}. \quad (8)$$

The corresponding SINR for the b-th Bob is expressed as [15],

$$\gamma_b^{\mathcal{B}}=\frac{\left|\mathbf{h}_b^{\mathcal{B}}\mathbf{w}_b^{\mathcal{B}}\right|^2}{\sum_{\substack{l=1\\l\neq b}}^{B}\left|\mathbf{h}_b^{\mathcal{B}}\mathbf{w}_l^{\mathcal{B}}\right|^2+\sum_{c=1}^{C}\left|\mathbf{h}_b^{\mathcal{B}}\mathbf{w}_c^{\mathcal{C}}\right|^2+\left|\left|\mathbf{h}_b^{\mathcal{RB}}\mathbf{\Theta}\right|\right|_2^2\sigma_{\mathcal{R}}^2+\sigma_b^{\mathcal{B}^2}}. \quad (9)$$

Thus, the achievable rate at Bob is given by

$$\mathcal{R}_b^{\mathcal{B}}=\log_2\left(1+\gamma_b^{\mathcal{B}}\right). \quad (10)$$

Achievable Rate at Carols: Similarly, the corresponding SINR for the c-th Carol can be written as

$$\gamma_c^{\mathcal{C}}=\frac{\left|\mathbf{h}_c^{\mathcal{C}}\mathbf{w}_c^{\mathcal{C}}\right|^2}{\sum_{b=1}^{B}\left|\mathbf{h}_c^{\mathcal{C}}\mathbf{w}_b^{\mathcal{B}}\right|^2+\sum_{\substack{l=1\\l\neq c}}^{C}\left|\mathbf{h}_c^{\mathcal{C}}\mathbf{w}_l^{\mathcal{C}}\right|^2+||\mathbf{h}_c^{\mathcal{RC}}\mathbf{\Theta}||_2^2\sigma_{\mathcal{R}}^2+\sigma_c^{\mathcal{C}^2}}. \quad (11)$$

Hence, the achievable rate at Carol is formulated as

$$\mathcal{R}_c^{\mathcal{C}}=\log_2\left(1+\gamma_c^{\mathcal{C}}\right). \quad (12)$$

D. Detection Performance at Willie

Applying the Neyman-Pearson (NP) test on the N samples of signal intercepted by Willie, the following hypothesis is envisaged:

$$y^{\mathcal{W}}(t)=\begin{cases}\mathbf{h}^{\mathcal{W}}\mathbf{W}^{\mathcal{C}}\mathbf{s}^{\mathcal{C}}(t)+\mathbf{h}^{\mathcal{W}}\mathbf{\Theta}\mathbf{z}_{\mathcal{R}}(t)+\mathbf{z}^{\mathcal{W}}(t), & \mathcal{H}_0\\ \mathbf{h}^{\mathcal{W}}\mathbf{W}^{\mathcal{B}}\mathbf{s}^{\mathcal{B}}(t)+\mathbf{h}^{\mathcal{W}}\mathbf{W}^{\mathcal{C}}\mathbf{s}^{\mathcal{C}}(t)+\mathbf{h}^{\mathcal{W}}\mathbf{\Theta}\mathbf{z}_{\mathcal{R}}(t)+\mathbf{z}^{\mathcal{W}}(t), & \mathcal{H}_1,\end{cases} \quad (13)$$

where $\mathbf{h}^{\mathcal{W}}=\left(\mathbf{h}^{\mathcal{AW}}+\mathbf{h}^{\mathcal{RW}}\mathbf{\Theta}\mathbf{G}\right) \in \mathbb{C}^{1\times N^2}$ represents the cascaded channel from Alice to Willie, and $z^{\mathcal{W}}(t) \sim \mathcal{CN}\left(0,\sigma^{\mathcal{W}^2}\right)$ denotes AWGN at Willie.

Applying the theory of a priori probability, the detection error probability (DEP) can be written in a more simplified form:

$$\xi \triangleq \mathbb{P}\left(\mathcal{D}_1|\mathcal{H}_0\right)+\mathbb{P}\left(\mathcal{D}_0|\mathcal{H}_1\right), \quad (14)$$

where $\mathcal{D}_1$ and $\mathcal{D}_0$ are the decisions in favor of $\mathcal{H}_1$ and $\mathcal{H}_0$, respectively.

Following the NP criterion, Willie performs a likelihood ratio test (LRT) leading to the decision rule:

$$\frac{\mathbb{P}_1\left(\mathbf{y}^{\mathcal{W}}|\mathcal{H}_1\right)}{\mathbb{P}_0\left(\mathbf{y}^{\mathcal{W}}|\mathcal{H}_0\right)} \underset{D_0}{\overset{D_1}{\gtrless}} \Gamma, \quad (15)$$

where Γ is a predetermined threshold the distributions under hypothesis $\mathcal{H}_0$ and $\mathcal{H}_1$ are expressed, respectively, as:

$$\mathbb{P}_0^{\mathcal{W}} \triangleq \mathbb{P}_0\left(\mathbf{y}^{\mathcal{W}}|\mathcal{H}_0\right) = \frac{\exp\left(-\frac{\left|\mathbf{y}^{\mathcal{W}}\right|^2}{\sum_{c=1}^{C}\left|\mathbf{h}^{\mathcal{W}}\mathbf{w}_c^{\mathcal{C}}\right|^2+||\mathbf{h}^{\mathcal{RW}}\mathbf{\Theta}||_2^2\sigma_{\mathcal{R}}^2+\sigma^{\mathcal{W}^2}}\right)}{\pi^N\left(\sum_{c=1}^{C}\left|\mathbf{h}^{\mathcal{W}}\mathbf{w}_c^{\mathcal{C}}\right|^2+\left|\left|\mathbf{h}^{\mathcal{RW}}\mathbf{\Theta}\right|\right|_2^2\sigma_{\mathcal{R}}^2+\sigma^{\mathcal{W}^2}\right)^N}, \quad (16)$$

$$\mathbb{P}_1^{\mathcal{W}} \triangleq \mathbb{P}_1\left(\mathbf{y}^{\mathcal{W}}|\mathcal{H}_1\right) = \frac{\exp\left(-\frac{\left|\mathbf{y}^{\mathcal{W}}\right|^2}{\sum_{b=1}^{B}\left|\mathbf{h}^{\mathcal{W}}\mathbf{w}_b^{\mathcal{B}}\right|^2+\sum_{c=1}^{C}\left|\mathbf{h}^{\mathcal{W}}\mathbf{w}_c^{\mathcal{C}}\right|^2+||\mathbf{h}^{\mathcal{RW}}\mathbf{\Theta}||_2^2\sigma_{\mathcal{R}}^2+\sigma^{\mathcal{W}^2}}\right)}{\pi^N\left(\sum_{b=1}^{B}\left|\mathbf{h}^{\mathcal{W}}\mathbf{w}_b^{\mathcal{B}}\right|^2+\sum_{c=1}^{C}\left|\mathbf{h}^{\mathcal{W}}\mathbf{w}_c^{\mathcal{C}}\right|^2+\left|\left|\mathbf{h}^{\mathcal{RW}}\mathbf{\Theta}\right|\right|_2^2\sigma_{\mathcal{R}}^2+\sigma^{\mathcal{W}^2}\right)^N}. \quad (17)$$

To ensure covertness, we apply the following KL-divergence constraint:

$$\mathcal{D}\left(\mathbb{P}_1^{\mathcal{W}}||\mathbb{P}_0^{\mathcal{W}}\right) \leq 2\epsilon^2, \quad (18)$$

which via Pinsker's inequality, guarantees that the total variation distance (TVD) remains below ϵ. Following the similar method to [16], the nonconvex expression (18) involving (16) and (17) can be simplified to the following equivalent covert constraint:

$$\Sigma_1-\left(1+\eta^{\mathcal{W}}\right)\Sigma_0 \leq \eta^{\mathcal{W}}\sigma^{\mathcal{W}^2}, \quad (19)$$

where $\eta^{\mathcal{W}} \geq 0$,

$$\Sigma_0=\sum_{c=1}^{C}\left|\mathbf{h}^{\mathcal{W}}\mathbf{w}_c^{\mathcal{C}}\right|^2+\left|\left|\mathbf{h}^{\mathcal{RW}}\mathbf{\Theta}\right|\right|_2^2\sigma_{\mathcal{R}}^2+\sigma^{\mathcal{W}^2}, \quad (20)$$

and

$$\Sigma_1=\sum_{b=1}^{B}\left|\mathbf{h}^{\mathcal{W}}\mathbf{w}_b^{\mathcal{B}}\right|^2+\sum_{c=1}^{C}\left|\mathbf{h}^{\mathcal{W}}\mathbf{w}_c^{\mathcal{C}}\right|^2+\left|\left|\mathbf{h}^{\mathcal{RW}}\mathbf{\Theta}\right|\right|_2^2\sigma_{\mathcal{R}}^2+\sigma^{\mathcal{W}^2}. \quad (21)$$

III. Channel Models

In this section, we present the channel models for Alice, Bob, Carol, and Willie, considering their respective antenna geometries. Alice, located at the origin, employs a UPA comprising $N\times N$ elements whose elements are indexed by n_x and n_y along the x and y axes, respectively, with indices defined as $n_x,n_y \in \{0,1,\cdots,(N-1)\}$. An inter-element distance d_A uniformly separates the elements along both axes, selected sufficiently large to prevent inter-element coupling. Further, we consider an active diagonal and planar $M\times M$ RIS located at (r_R,θ_R,ϕ_R), whose diagonal elements are indexed by $m \in \{0,1,\cdots,(M-1)\}$, with a large diagonal element spacing of d_R. Finally, Bob, Carol, and Willie each utilize a single antenna element and are located at (r_b,θ_b,ϕ_b), (r_c,θ_c,ϕ_c) and $\left(r^{\mathcal{W}},\theta^{\mathcal{W}},\phi^{\mathcal{W}}\right)$, respectively.

A. Alice-to-Bob line-of-sight (LOS) Channel Model

NF Channel: Let the direct LOS channel from Alice to the b-th Bob be denoted by the channel vector $\mathbf{h}_b^{\mathcal{AB}} \in \mathbb{C}^{1\times N^2}$. The path difference from the (n_x,n_y)-th and $(0,0)$-th antenna element of Alice to the b-th Bob can be approximated by Taylor's series approximation to obtain:

$$\Delta r_{b,(n_x,n_y)}^{\mathcal{AB}} \approx -\left(n_x d_A\chi_b^X+n_y d_A\chi_b^Y\right) + \frac{1}{2r_b}\left\{n_x^2d_A^2\left(1-\chi_b^{X^2}\right)+n_y^2d_A^2\left(1-\chi_b^{Y^2}\right)-2n_xn_yd_A^2\chi_b^X\chi_b^Y\right\}, \quad (22)$$

where $\chi_b^X=\sin\theta_b\cos\phi_b$ and $\chi_b^Y=\sin\theta_b\cos\phi_b$. The corresponding beamfocusing vector can be written as:

$$\mathbf{a}^{\mathcal{AB}}(r_b,\theta_b,\phi_b)=\frac{1}{\sqrt{N^2}}\exp\left(-j\frac{2\pi}{\lambda}\mathbf{\Delta r}_{\mathbf{b}}^{\mathcal{AB}}\right), \quad (23)$$

where $\mathbf{\Delta r}_{\mathbf{b}}^{\mathcal{AB}}$ is the path difference vector and λ is the operating wavelength. Applying the Fresnel approximation across the transmit array yields the NF channel vector

$$\mathbf{h}_b^{\mathcal{A}}=\frac{1}{\sqrt{N^2}}\frac{1}{\sqrt{4\pi r_b^2}}\exp\left[-j\frac{2\pi}{\lambda}r_b\right]\mathbf{a}^{\mathcal{AB}}(r_b,\theta_b,\phi_b). \quad (24)$$

B. Alice-to-RIS Channel Model

NF Channel: Similar approximation for Alice-to-RIS channel yields the corresponding approximation for path difference:

$$\Delta r^{\mathcal{AR}}_{m,(n_x,n_y)} \approx \left(X_R\chi^X_R + Y_R\chi^Y_R\right) + \frac{1}{2r_R}\left\{X^2_R\left(1-\chi^{X^2}_R\right)+Y_R\left(1-\chi^{Y^2}_R\right)-2X_RY_R\chi^X_R\chi^Y_R\right\}, \quad (25)$$

where $\chi^X_R = \sin\theta_R\cos\phi_R$, $\chi^Y_R = \sin\theta_R\sin\phi_R$, $X_R = (md_R - n_xd_A)$, and $Y_R = (md_R - n_yd_A)$. Therefore, the corresponding beamsteering matrix is written as

$$\mathbf{A} = \frac{1}{\sqrt{MN^2}}\exp\left[-j\frac{2\pi}{\lambda}\mathbf{\Delta R}^{\mathcal{AR}}\right]. \quad (26)$$

Under the Fresnel approximation, the NF channel from Alice to RIS is given by

$$\mathbf{G} = \frac{1}{\sqrt{MN^2}}\frac{1}{\sqrt{4\pi r^2_R}}\exp\left[-j\frac{2\pi}{\lambda}r_R\right]\mathbf{A}. \quad (27)$$

C. RIS-to-Bob Channel Model

NF Channel: To formulate the RIS-to-receiver channel, Bob's location (r_b, θ_b, ϕ_b) is geometrically translated to the RIS's local coordinate system, resulting in a new spherical coordinate $\left(\overline{r}_b, \overline{\theta}_b, \overline{\phi}_b\right)$. The corresponding expression for the approximate path difference is given by,

$$\Delta\overline{r}^{\mathcal{RB}}_{b,m} \approx -md_R\left(\overline{\chi}^X_b + \overline{\chi}^Y_b\right) + \frac{m^2d^2_R}{2\overline{r}_b}\left\{\left(1-\overline{\chi}^{X^2}_b\right)+\left(1-\overline{\chi}^{Y^2}_b\right)-2\overline{\chi}^X_b\overline{\chi}^Y_b\right\}, \quad (28)$$

where $\overline{\chi}^X_b = \sin\overline{\theta}_b\cos\overline{\phi}_b$ and $\overline{\chi}^Y_b = \sin\overline{\theta}_b\sin\overline{\phi}_b$.

Using (28), the beamfocusing vector is expressed as

$$\overline{\mathbf{a}}^{\mathcal{RB}}\left(\overline{r}_b, \overline{\theta}_b, \overline{\phi}_b\right) = \frac{1}{\sqrt{M}}\exp\left(-j\frac{2\pi}{\lambda}\mathbf{\Delta}\overline{\mathbf{r}}^{\mathcal{RB}}_{\mathbf{b}}\right), \quad (29)$$

where $\mathbf{\Delta}\overline{\mathbf{r}}^{\mathcal{RB}}_{\mathbf{b}} \in \mathbb{R}^{1\times M}$ is the vector containing the elements (28). Consequently, applying the Fresnel approximation, the NF RIS-to-receiver channel vector is derived as

$$\mathbf{h}^{\mathcal{RB}}_b = \frac{1}{\sqrt{M}}\frac{1}{\sqrt{4\pi\overline{r}^2_b}}\exp\left[-j\frac{2\pi}{\lambda}\right]\overline{\mathbf{a}}^{\mathcal{RB}}\left(\overline{r}_b, \overline{\theta}_b, \overline{\phi}_b\right). \quad (30)$$

D. Willie's Bounded-Error CSI Model

This section considers the bounded CSI error model for Willie [7]. Specifically, the true channel is assumed to lie in an ℓ_2-ball around its estimate.

$$\mathbf{h}^{\mathcal{AW}} = \hat{\mathbf{h}}^{\mathcal{AW}} + \Delta\mathbf{h}^{\mathcal{AW}}, \quad \left|\left|\Delta\mathbf{h}^{\mathcal{AW}}\right|\right|_2 \le \varepsilon^{\mathcal{AW}}, \quad (31)$$

$$\mathbf{h}^{\mathcal{RW}} = \hat{\mathbf{h}}^{\mathcal{RW}} + \Delta\mathbf{h}^{\mathcal{RW}}, \quad \left|\left|\Delta\mathbf{h}^{\mathcal{RW}}\right|\right|_2 \le \varepsilon^{\mathcal{RW}}, \quad (32)$$

where $\varepsilon^{\mathcal{AW}}$ and $\varepsilon^{\mathcal{RW}}$ represent the error bounds. This bounded-error characterization enables covertness constraint derivations via suitable approximations discussed in the following sections.

E. Covert Constraint at Willie

Adopting the bounded channel error at Willie, we can rewrite Σ_0 and Σ_1 from (20) and (21), respectively, in the constraint form:

$$\Sigma_0 \ge \left[\max\left(\left|\left|\hat{\mathbf{h}}^{\mathcal{W}}\mathbf{W_C}\right|\right| + \left|\left|\hat{\mathbf{h}}^{\mathcal{RW}}\mathbf{\Theta}\right|\right|\sigma_{\mathcal{R}} + \sigma^{\mathcal{W}} - \varepsilon^{\mathcal{AW}}||\mathbf{W_C}|| - \varepsilon^{\mathcal{RW}}||\mathbf{\Theta G W_C}|| - \varepsilon^{\mathcal{RW}}||\mathbf{\Theta}||\sigma_{\mathcal{R}}, 0\right)\right]^2,$$

$$\Sigma_1 \le \left[\left|\left|\hat{\mathbf{h}}^{\mathcal{W}}\mathbf{W_{B,C}}\right|\right| + \left|\left|\hat{\mathbf{h}}^{\mathcal{RW}}\mathbf{\Theta}\right|\right|\sigma_{\mathcal{R}} + \sigma^{\mathcal{W}} + \varepsilon^{\mathcal{AW}}||\mathbf{W_{B,C}}|| + \varepsilon^{\mathcal{RW}}||\mathbf{\Theta G W_{B,C}}|| + \varepsilon^{\mathcal{RW}}||\mathbf{\Theta}||\sigma_{\mathcal{R}}\right]^2. \quad (33)$$

where $\mathbf{W_C} = \left[\mathbf{w}^{\mathcal{C}}_1, \cdots, \mathbf{w}^{\mathcal{C}}_C\right]$, and $\mathbf{W_{B,C}} = \left[\mathbf{w}^{\mathcal{B}}_1, \cdots, \mathbf{w}^{\mathcal{B}}_B; \mathbf{w}^{\mathcal{C}}_1, \cdots, \mathbf{w}^{\mathcal{C}}_C\right]$.

IV. Problem Formulation and Proposed Solution

Our objective is to maximize the sum of achievable throughput rates for all the covert and overt users, subject to constraints on minimum rate QoS, total transmit power budgets, and covert constraints requirements. The optimization problem is formulated as

$$(\boldsymbol{\mathcal{P}1}) \quad \max_{\mathbf{W}^{\mathcal{B}},\mathbf{W}^{\mathcal{C}},\mathbf{\Theta}} \quad \sum\nolimits_{b=1}^{B}\omega^{\mathcal{B}}_b\mathcal{R}^{\mathcal{B}}_b + \sum\nolimits_{c=1}^{C}\omega^{\mathcal{C}}_c\mathcal{R}^{\mathcal{C}}_c \quad (34)$$

$$\text{s.t.} \quad (\boldsymbol{\mathcal{C}1}) \quad 0 \le \mathcal{R}^{\mathcal{B}}_{min} \le \mathcal{R}^{\mathcal{B}}_b, \quad \forall\, b \in \mathbf{B}$$

$$(\boldsymbol{\mathcal{C}2}) \quad 0 \le \mathcal{R}^{\mathcal{C}}_{min} \le \mathcal{R}^{\mathcal{C}}_c, \quad \forall\, c \in \mathbf{C}$$

$$(\boldsymbol{\mathcal{C}3}) \quad (4), (5), \text{ and } (6),$$

$$(\boldsymbol{\mathcal{C}4}) \quad (19),$$

where $\mathcal{R}^{\mathcal{B}}_{min}$ and $\mathcal{R}^{\mathcal{C}}_{min}$ denotes the Bobs and Carols minimum required rate. The presented problem $\boldsymbol{\mathcal{P}1}$ is non-convex due to the not only tight coupling between the RIS reflection matrix $\mathbf{\Theta}$ and the beamforming vectors $\mathbf{W}^{\mathcal{B}}$ and $\mathbf{W}^{\mathcal{C}}$ but also due to the nonlinear fractional rate expressions, RIS-related power and amplification constraints, and thus, requires a tractable transformation for solving through convex optimization.

A. Convex Reformulation of the Joint Beamforming Design

The objective function is linearized by introducing auxiliary variables $\{t^{\mathcal{B}}_b\}_{\forall b\in\mathbf{B}}$ and $\{t^{\mathcal{C}}_c\}_{\forall c\in\mathbf{C}}$, and thereafter rewriting it as:

$$\max_{\mathbf{W}^{\mathcal{B}},\mathbf{W}^{\mathcal{C}},\mathbf{\Theta},\mathbf{t}^{\mathcal{B}},\mathbf{t}^{\mathcal{C}}} \quad \sum\nolimits_{b=1}^{B}\omega^{\mathcal{B}}_b t^{\mathcal{B}}_b + \sum\nolimits_{c=1}^{C}\omega^{\mathcal{C}}_c t^{\mathcal{C}}_c, \quad (35)$$

which is convex and thus, transform the constraints $\boldsymbol{\mathcal{C}1}$ and $\boldsymbol{\mathcal{C}2}$ into the convex form:

$$0 \le \mathcal{R}^{\mathcal{B}}_{min} \le t^{\mathcal{B}}_b + p^1_b, \quad (36)$$

$$0 \le \mathcal{R}^{\mathcal{C}}_{min} \le t^{\mathcal{C}}_c + p^2_c, \quad (37)$$

where p^1_b and p^2_b represents the concerned penalty. However, to convexify the inequality $t^{\mathcal{B}}_b \le \mathcal{R}^{\mathcal{B}}_b$ introduced as a consequence of reformulating the objective function, we define auxiliary variables $u^{\mathcal{B}}_b$ and $v^{\mathcal{B}}_b$ and rewrite the inequality as:

$$v^{\mathcal{B}}_b \le \frac{{u^{\mathcal{B}}_b}^2}{2^{t^{\mathcal{B}}_b}-1}, \quad (38)$$

which is approximated via a first-order Taylor expansion around the previous iterative solution $\left(\underline{t}^{\mathcal{B}}_b, \underline{u}^{\mathcal{B}}_b\right)$ to obtain a convex surrogate with added penalty variable p^3_b, written as

$$v^{\mathcal{B}}_b \le \frac{{u^{\mathcal{B}}_b}^2}{2^{\underline{t}^{\mathcal{B}}_b}-1} + \left(u^{\mathcal{B}}_b - \underline{u}^{\mathcal{B}}_b\right)\frac{2\underline{u}^{\mathcal{B}}_b}{2^{\underline{t}^{\mathcal{B}}_b}-1} + \left(t^{\mathcal{B}}_b - \underline{t}^{\mathcal{B}}_b\right)\frac{\underline{u}^{\mathcal{B}}_b 2^{\underline{t}^{\mathcal{B}}_b}\log 2}{\left(2^{\underline{t}^{\mathcal{B}}_b}-1\right)^2} + p^3_b. \quad (39)$$

In constraint $\boldsymbol{\mathcal{C}2}$, the same convexification procedure is applied to obtain a similar rate expression associated with Carols.

Under the alternating optimization (AO) framework, the RIS amplification constraint $\boldsymbol{\mathcal{C}3}$ is handled in two stages. When optimizing $\left(\mathbf{W}^{\mathcal{B}}, \mathbf{W}^{\mathcal{C}}\right)$ with fixed $\mathbf{\Theta}$, constraint (4) becomes irrelevant and is excluded. However, during $\mathbf{\Theta}$ update, it is split into:

$$|\phi_m| \le \eta^{\mathcal{R}} + p^4_m, \quad (40)$$

$$1 \le |\phi_m|, \quad (41)$$

where (40) is convex, and p_m^4 represents the penalty. However, (41) is convexified using the first-order approximation of its right-hand side to obtain:

$$1 \leq \left|\underline{\phi}_m\right| + \Re\left\{\frac{\underline{\phi}_m^*}{\left|\underline{\phi}_m\right|}(\phi_m - \underline{\phi}_m)\right\} + p_m^5, \tag{42}$$

with p_m^5 denoting the penalty variable.

To convexify the covertness constraint $\boldsymbol{C4}$, we introduce slack variables $u^{\mathcal{W}} \geq 0$ and $v^{\mathcal{W}} \geq 0$, reformulating the original nonconvex constraint (19) and then applying Taylor's approximation to linearize the constraint as follows:

$$u^{\mathcal{W}^2} \leq \eta^{\mathcal{W}}\sigma^{\mathcal{W}^2} + \left(1+\eta^{\mathcal{W}}\right)\left(\underline{v}^{\mathcal{W}}v^{\mathcal{W}} - \left|\underline{v}^{\mathcal{W}}\right|^2\right) + p^6, \tag{43}$$

further introducing the following two SOCP constraints under robust formulations:

$$\begin{aligned} v^{\mathcal{W}} \leq & \left|\left|\hat{\mathbf{h}}^{\mathcal{A}\mathcal{W}}\mathbf{W_C}\right|\right| + \left|\left|\hat{\mathbf{h}}^{\mathcal{R}\mathcal{W}}\boldsymbol{\Theta}\mathbf{G}\mathbf{W_C}\right|\right| + \left|\left|\hat{\mathbf{h}}^{\mathcal{R}\mathcal{W}}\boldsymbol{\Theta}\right|\right|\sigma_{\mathcal{R}} \\ & + \sigma^{\mathcal{W}} - \varepsilon^{\mathcal{A}\mathcal{W}}\left|\left|\mathbf{W_C}\right|\right| - \varepsilon^{\mathcal{R}\mathcal{W}}\left|\left|\boldsymbol{\Theta}\mathbf{G}\mathbf{W_C}\right|\right| - \varepsilon^{\mathcal{R}\mathcal{W}}\left|\left|\boldsymbol{\Theta}\right|\right|\sigma_{\mathcal{R}} + p^7 \\ & \left|\left|\hat{\mathbf{h}}^{\mathcal{A}\mathcal{W}}\mathbf{W_{B,C}}\right|\right| + \left|\left|\hat{\mathbf{h}}^{\mathcal{R}\mathcal{W}}\boldsymbol{\Theta}\mathbf{G}\mathbf{W_{B,C}}\right|\right| + \left|\left|\hat{\mathbf{h}}^{\mathcal{R}\mathcal{W}}\boldsymbol{\Theta}\right|\right|\sigma_{\mathcal{R}} \\ & \sigma^{\mathcal{W}} + \varepsilon^{\mathcal{A}\mathcal{W}}\left|\left|\mathbf{W}_{B,C}\right|\right| \leq u^{\mathcal{W}} + p^8, \end{aligned} \tag{44}$$

which can be made convex by applying the following approximations for $||\cdot||$ given by

$$||A|| = ||\underline{A}|| + \frac{1}{||\underline{A}||}\Re\boldsymbol{Tr}\left\{A^H\left(A - \underline{A}\right)\right\}. \tag{45}$$

Since all the constraints are transformed into a convex form, the subproblem for beamforming optimization is written as

$$\begin{aligned} (\boldsymbol{P2}) \quad & \max_{\substack{\mathbf{W}^{\mathcal{B}},\mathbf{W}^{\mathcal{C}},\mathbf{t}^{\mathcal{B}},\mathbf{t}^{\mathcal{C}},\mathbf{u}^{\mathcal{B}},\\ \mathbf{v}^{\mathcal{B}},\mathbf{u}^{\mathcal{C}},\mathbf{v}^{\mathcal{C}},u^{\mathcal{W}},v^{\mathcal{W}}}} \sum\nolimits_{b=1}^{B}\omega_b^{\mathcal{B}}t_b^{\mathcal{B}} + \sum\nolimits_{c=1}^{C}\omega_c^{C}t_c^{\mathcal{C}} - \lambda^{\mathcal{P}}\left|\left|\overline{\mathbf{p}}\right|\right| \\ \text{s.t.} \quad & (5), (6), (36), (37), (39), (43), \text{ and } (44). \end{aligned} \tag{46}$$

where $\lambda^{\mathcal{P}} \geq 1$ is a suitable value of penalty which balances the objective vs. constraint violations; $\overline{\mathbf{p}} = \left[\left\{p_b^1, p_b^3,\right\}_{\forall \mathbf{B}}, \left\{p_c^2, p_c^3,\right\}_{\forall \mathbf{C}}, p^6, p^7, p^8\right]$ are a collection of penalty variable which are driven to zero at the optimum. The problem is now convex in $\mathbf{W_{B,C}}$ and therefore can be solved with any off-the-shelf convex solver.

Similarly, the RIS-update subproblem can be formulated as follows:

$$\begin{aligned} (\boldsymbol{\mathcal{P}3}) \quad & \max_{\substack{\boldsymbol{\Theta},\mathbf{t}^{\mathcal{B}},\mathbf{t}^{\mathcal{C}},\mathbf{u}^{\mathcal{B}},\\ \mathbf{v}^{\mathcal{B}},\mathbf{u}^{\mathcal{C}},\mathbf{v}^{\mathcal{C}},u^{\mathcal{W}},v^{\mathcal{W}}}} \sum\nolimits_{b=1}^{B}\omega_b^{\mathcal{B}}t_b^{\mathcal{B}} + \sum\nolimits_{c=1}^{C}\omega_c^{C}t_c^{\mathcal{C}} - \lambda^{\mathcal{P}}\left|\left|\overline{\mathbf{p}}\right|\right| \\ \text{s.t.} \quad & (6), (36), (37), (39), (40), (42), (43), \text{ and } (44), \end{aligned} \tag{47}$$

is a convex problem where $\lambda^{\mathcal{P}} \geq 1$ is a suitable value of penalty: $\overline{\mathbf{p}} = \left[\left\{p_b^1, p_b^3,\right\}_{\forall \mathbf{B}}, \left\{p_c^2, p_c^3\right\}_{\forall \mathbf{C}}, \left\{p_m^4, p_m^5\right\}_{\forall \mathbf{M}}, p^6, p^7, p^8\right]$ are a collection of penalty variable which attains zero at the optimal point. The problem listed is now convex and can be solved with any interior point solver. However, to jointly optimize the RIS reflection vector and the beamforming vector, the **Algorithm 1** is executed iteratively until convergence is attained.

V. Numerical Results

In this section, we present the numerical results to evaluate the performance of our proposed algorithm for the RIS-aided covert communication framework under the eavesdropper's imperfect CSI in NF propagation conditions. Table I summarizes all key simulation and solver parameters used throughout our simulations, including the 24 GHz carrier frequency, antenna array geometries (4×4 at the BS, 16 elements at the RIS), path-loss exponents, noise and channel uncertainty levels, node positions, minimum rate, and covertness requirements. Figure 2 illustrates the convergence of the weighted sum-rate for both Bobs and Carols versus iteration number under NF and FF models. In the NF regime, the proposed AO scheme initially converges more slowly, lagging behind both the PSO-based and random RIS baselines for the first 200 iterations but thereafter surpasses them, achieving the highest sum-rate for all subsequent iterations. The random RIS outperforms the PSO approach up to roughly 310 iterations, after which PSO regains superiority over the random baseline. By contrast, FF operation yields substantially lower sum-rates throughout the entire convergence process, reflecting the loss of spatial focusing and unfavorable path loss characteristics. These results underscore the critical importance of jointly optimizing RIS phase profiles and beamformers in the NF, where enhanced spatial resolution and path loss advantages can be fully exploited to maximize system throughput.

Algorithm 1: Unified beamforming and RIS optimization

Initialize $\left[\underline{\mathbf{W}}^{\mathcal{B}},\underline{\mathbf{W}}^{\mathcal{C}},\underline{\boldsymbol{\Theta}},\mathbf{t}^{\mathcal{B}},\mathbf{u}^{\mathcal{B}},\mathbf{v}^{\mathcal{B}},\mathbf{t}^{\mathcal{C}},\mathbf{u}^{\mathcal{C}},\mathbf{v}^{\mathcal{C}},u^{\mathcal{W}},v^{\mathcal{W}}\right]$, μ^{up}, $\lambda^{\mathcal{P}}$;
counter $n \leftarrow 0$;
while *not converged* **do**
  $\left[\mathbf{W}^{\mathcal{B}},\mathbf{W}^{\mathcal{C}},\mathbf{t}^{\mathcal{B}},\mathbf{u}^{\mathcal{B}},\mathbf{v}^{\mathcal{B}},\mathbf{t}^{\mathcal{C}},\mathbf{u}^{\mathcal{C}},\mathbf{v}^{\mathcal{C}},u^{\mathcal{W}},v^{\mathcal{W}}\right]^{(a)} \leftarrow$
  $\boldsymbol{\mathcal{P}2}(\left[\mathbf{W}^{\mathcal{B}},\mathbf{W}^{\mathcal{C}},\boldsymbol{\Theta},\mathbf{t}^{\mathcal{B}},\mathbf{u}^{\mathcal{B}},\mathbf{v}^{\mathcal{B}},\mathbf{t}^{\mathcal{C}},\mathbf{u}^{\mathcal{C}},\mathbf{v}^{\mathcal{C}},u^{\mathcal{W}},v^{\mathcal{W}}\right]^{(n)},\lambda^{\mathcal{P}})$;
  $\left[\mathbf{W}^{\mathcal{B}},\mathbf{W}^{\mathcal{C}},\mathbf{t}^{\mathcal{B}},\mathbf{u}^{\mathcal{B}},\mathbf{v}^{\mathcal{B}},\mathbf{t}^{\mathcal{C}},\mathbf{u}^{\mathcal{C}},\mathbf{v}^{\mathcal{C}},u^{\mathcal{W}},v^{\mathcal{W}}\right]^{(n)} +=$
  $\mu^{\text{up}} \times \left(\left[\mathbf{W}^{\mathcal{B}},\mathbf{W}^{\mathcal{C}},\mathbf{t}^{\mathcal{B}},\mathbf{u}^{\mathcal{B}},\mathbf{v}^{\mathcal{B}},\mathbf{t}^{\mathcal{C}},\mathbf{u}^{\mathcal{C}},\mathbf{v}^{\mathcal{C}},u^{\mathcal{W}},v^{\mathcal{W}}\right]^{(a)}\right.$
  $\left.-\left[\mathbf{W}^{\mathcal{B}},\mathbf{W}^{\mathcal{C}},\mathbf{t}^{\mathcal{B}},\mathbf{u}^{\mathcal{B}},\mathbf{v}^{\mathcal{B}},\mathbf{t}^{\mathcal{C}},\mathbf{u}^{\mathcal{C}},\mathbf{v}^{\mathcal{C}},u^{\mathcal{W}},v^{\mathcal{W}}\right]^{(n)}\right)$;
  $\left[\boldsymbol{\Theta},\mathbf{t}^{\mathcal{B}},\mathbf{u}^{\mathcal{B}},\mathbf{v}^{\mathcal{B}},\mathbf{t}^{\mathcal{C}},\mathbf{u}^{\mathcal{C}},\mathbf{v}^{\mathcal{C}},u^{\mathcal{W}},v^{\mathcal{W}}\right]^{(b)} \leftarrow$
  $\boldsymbol{\mathcal{P}3}(\left[\mathbf{W}^{\mathcal{B}},\mathbf{W}^{\mathcal{C}},\boldsymbol{\Theta},\mathbf{t}^{\mathcal{B}},\mathbf{u}^{\mathcal{B}},\mathbf{v}^{\mathcal{B}},\mathbf{t}^{\mathcal{C}},\mathbf{u}^{\mathcal{C}},\mathbf{v}^{\mathcal{C}},u^{\mathcal{W}},v^{\mathcal{W}}\right]^{(n)},\lambda^{\mathcal{P}})$;
  $\left[\boldsymbol{\Theta},\mathbf{t}^{\mathcal{B}},\mathbf{u}^{\mathcal{B}},\mathbf{v}^{\mathcal{B}},\mathbf{t}^{\mathcal{C}},\mathbf{u}^{\mathcal{C}},\mathbf{v}^{\mathcal{C}},u^{\mathcal{W}},v^{\mathcal{W}}\right]^{(n)} +=$
  $\mu^{\text{up}} \times \left(\left[\boldsymbol{\Theta},\mathbf{t}^{\mathcal{B}},\mathbf{u}^{\mathcal{B}},\mathbf{v}^{\mathcal{B}},\mathbf{t}^{\mathcal{C}},\mathbf{u}^{\mathcal{C}},\mathbf{v}^{\mathcal{C}},u^{\mathcal{W}},v^{\mathcal{W}}\right]^{(b)}\right.$
  $\left.-\left[\boldsymbol{\Theta},\mathbf{t}^{\mathcal{B}},\mathbf{u}^{\mathcal{B}},\mathbf{v}^{\mathcal{B}},\mathbf{t}^{\mathcal{C}},\mathbf{u}^{\mathcal{C}},\mathbf{v}^{\mathcal{C}},u^{\mathcal{W}},v^{\mathcal{W}}\right]^{(n)}\right)$;
  $\left[\mathbf{W}^{\mathcal{B}},\mathbf{W}^{\mathcal{C}},\boldsymbol{\Theta},\mathbf{t}^{\mathcal{B}},\mathbf{u}^{\mathcal{B}},\mathbf{v}^{\mathcal{B}},\mathbf{t}^{\mathcal{C}},\mathbf{u}^{\mathcal{C}},\mathbf{v}^{\mathcal{C}},u^{\mathcal{W}},v^{\mathcal{W}}\right]^{(n+1)} \leftarrow$
  $\left[\mathbf{W}^{\mathcal{B}},\mathbf{W}^{\mathcal{C}},\boldsymbol{\Theta},\mathbf{t}^{\mathcal{B}},\mathbf{u}^{\mathcal{B}},\mathbf{v}^{\mathcal{B}},\mathbf{t}^{\mathcal{C}},\mathbf{u}^{\mathcal{C}},\mathbf{v}^{\mathcal{C}},u^{\mathcal{W}},v^{\mathcal{W}}\right]^{(n)}$;
  $n \leftarrow n+1$;
return $\mathbf{W}^{\mathcal{B}}$, $\mathbf{W}^{\mathcal{C}}$, $\boldsymbol{\Theta}$

TABLE I: Key Simulation and Solver Parameters

Parameter	Value
System Configuration	
Operating frequency	24 GHz
Total power (Alice, RIS)	40 dBm
Alice array size	4×4, spacing 0.50 m
RIS array	16 el., spacing 0.10, amp. factor 1000
Path-loss exponents	Alice→Rx: 3.0; RIS: 2.2. RIS→Rx: 2.0
Noise variance (σ^2)	10^{-4}
Channel uncertainty	Alice→Bob: 10^{-5}; others: 10^{-4}
Covertness ϵ (Willie)	0.10
Node Positions (X, Y, Z) [m]	
Alice	(0, 0, 0)
RIS	(0, 0, 3)
Bob	(5, 5, 1), (10, 5, 0), (12, 1, 0), (14, 3, 0), (14, 4, 1)
Carol	(7, 0, 0), (8, 5, 1), (18, 3, 1)

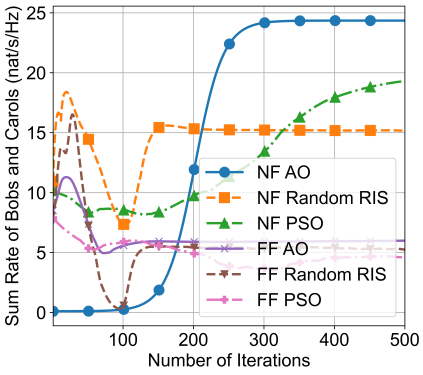

Fig. 2: Convergence plot of Weighted sum-rate.

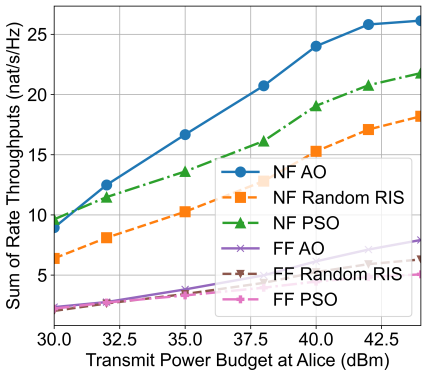

Fig. 3: Sum throughput versus transmit-power.

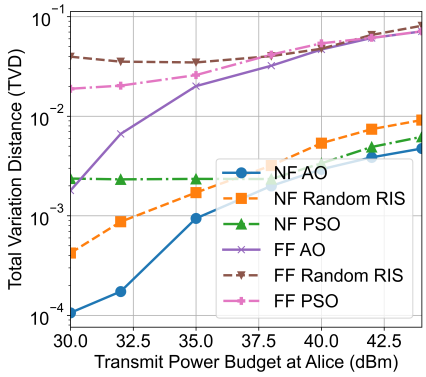

Fig. 4: TVD variation with transmit-power budget.

Fig. 3 illustrates the sum of the rate throughput for Alice's transmit power budget. As the transmit power increases, all schemes exhibit improved throughput performance. Specifically for NF, the proposed AO approach achieves a throughput of approximately 24 nat/s/Hz at 40 dBm, outperforming both the PSO and random RIS. In contrast, all FF-based schemes exhibit a substantial reduction in throughput, primarily due to weaker spatial selectivity and reduced RIS effectiveness. These findings highlight the critical role of NF-RIS design and optimization in achieving high-throughput covert communications, particularly under stringent power constraints.

Fig. 4 presents the TVD versus Alice's transmit-power budget, highlighting the impact of power allocation on the detectability of covertness. In FF-based scenarios, all benchmark schemes exhibit a pronounced rise in TVD as transmit power increases, signifying degraded covertness. In contrast, NF transmission benefits from enhanced spatial focusing, which effectively suppresses covert signal leakage and improves stealth performance. Notably, the AO-based design consistently achieves the lowest TVD across all power levels, validating the efficacy of our joint beamforming and active RIS reflection strategy in minimizing detectability. Furthermore, unoptimized RIS configurations (Random RIS) significantly deteriorate covertness, while PSO-based optimization yields moderate gains but remains inferior to AO, highlighting the limitations of meta-heuristic methods in precision-critical covert communication tasks.

VI. Conclusion

In this work, we proposed a joint beamforming and active RIS reflection design for integrated overt–covert communication in NF 6G networks under bounded CSI uncertainty. By modeling the warden's channel with an ℓ_2-bounded error and enforcing a KL-divergence-based covertness constraint, we reformulated the sum-rate maximization problem into a sequence of SOCPs, solved via AO with SCA and trust-region penalization. Our active RIS design enables joint phase and amplitude control, achieving a throughput of 24 nat/s/Hz and maintains a low TVD across diverse power budgets. Compared to passive RIS and FF-based scenarios, the proposed method delivers over threefold performance improvement.

References

[1] A. Mukhopadhyay, K. Singh, F.-S. Tseng, S. K. Singh, K. Dev, and C. Pan, "A tutorial on near-field driven 6G networks," *IEEE Commun. Surv. Tut.*, pp. 1–1, Mar. (early) 2025.

[2] S. Pala, K. Singh, O. Taghizadeh, C. Pan, O. A. Dobre, and T. Q. Duong, "Robust and secure multi-user STAR-RIS-aided communications: Optimization vs machine learning," *IEEE Trans. Commun.*, pp. 1–1, Feb. (early) 2025.

[3] B. A. Bash, D. Goeckel, and D. Towsley, "Limits of reliable communication with low probability of detection on AWGN channels," *IEEE J. Sel. Areas Commun.*, vol. 31, no. 9, pp. 1921–1930, Sep. 2013.

[4] L. Wang, G. W. Wornell, and L. Zheng, "Fundamental limits of communication with low probability of detection," *IEEE Trans. Inf. Theory*, vol. 62, no. 6, pp. 3493–3503, Jun. 2016.

[5] H. ZivariFard and X. Wang, "Covert communication via action-dependent states," *IEEE Trans. Inf. Theory*, vol. 71, no. 4, pp. 3100–3128, Apr. 2025.

[6] Y. Zhang *et al.*, "Covert communication in downlink NOMA systems with channel uncertainty," *IEEE Sensors J.*, vol. 22, no. 19, pp. 19 101–19 112, Oct. 2022.

[7] R. Tang, L. Yang, L. Lv, Z. Zhang, Y. Liu, and J. Chen, "Dual-functional artificial noise (DFAN) aided robust covert communications in integrated sensing and communications," *IEEE Trans. Commun.*, vol. 73, no. 2, pp. 1072–1086, Feb. 2025.

[8] J. Wang, W. Tang, Q. Zhu, X. Li, H. Rao, and S. Li, "Covert communication with the help of relay and channel uncertainty," *IEEE Wireless Commun. Lett.*, vol. 8, no. 1, pp. 317–320, Feb. 2019.

[9] J. Si, Z. Liu, Z. Li, H. Hu, L. Guan, C. Wang, and N. Al-Dhahir, "A cooperative deception strategy for covert communication in presence of a multi-antenna adversary," *IEEE Trans. Commun.*, vol. 71, no. 8, pp. 4778–4792, Aug. 2023.

[10] S. Singh, R. Allu, K. Singh, S. K. Singh, and M.-L. Ku, "Green multi-active RIS-aided secure full-duplex IoT networks with imperfect CSI: A power minimization approach," *IEEE Internet Things J.*, pp. 1–1, Apr. 2025.

[11] M. Di Renzo *et al.*, "Smart Radio Environments empowered by Reconfigurable Intelligent Surfaces: How it works, state of research, and the road ahead," *IEEE J. Sel. Areas Commun.*, vol. 38, no. 11, pp. 2450–2525, Nov. 2020.

[12] S. Singh, A. Raviteja, K. Singh, S. K. Singh, A. Kaushik, and M.-L. Ku, "Secrecy rate maximization for active ris-aided robust uplink noma communications," *IEEE Wireless Commun. Lett.*, vol. 13, no. 11, pp. 2960–2964, Nov. 2024.

[13] J. An, C. Yuen, L. Dai, M. Di Renzo, M. Debbah, and L. Hanzo, "Near-field communications: Research advances, potential, and challenges," *IEEE Wireless Commun.*, vol. 31, no. 3, pp. 100–107, Jun. 2024.

[14] F. Shu and J. Wang, *Intelligent Reflecting Surface-Aided Physical-Layer Security*, 1st ed. Cham, Switzerland: Springer, 2023.

[15] M. Zhu, F. Lu, X. Kang, P. Chen, G. Pan, and H. Liu, "Active-RIS-aided covert communications in NOMA-inspired ISAC systems," in *Proc. ICCC Workshops*. Hangzhou, China: IEEE, Aug. 2024, pp. 811–816.

[16] J. Hu, Y. Zhou, H. Zheng, F. Shu, and J. Wang, "Minimizing Vulnerable Region for Near-Field Covert Communication," *IEEE Trans. Veh. Technol.*, vol. 73, no. 12, pp. 19 861–19 866, Dec. 2024.